



**HAL**  
open science

## Implementation of an imaging spectrometer for localization and identification of radioactive sources

H. Lemaire, R. Abou Khalil, K. Amgarou, J.C. Angélique, Fabrice Bonnet, D.  
de Toro, F. Carrel, O. Giarmana, M. Gmar, N. Menaa, et al.

### ► To cite this version:

H. Lemaire, R. Abou Khalil, K. Amgarou, J.C. Angélique, Fabrice Bonnet, et al.. Implementation of an imaging spectrometer for localization and identification of radioactive sources. Nuclear Instruments and Methods in Physics Research Section A: Accelerators, Spectrometers, Detectors and Associated Equipment, 2014, 763, pp.97-103. 10.1016/j.nima.2014.05.118 . in2p3-01024125

**HAL Id: in2p3-01024125**

**<https://hal.in2p3.fr/in2p3-01024125>**

Submitted on 20 Mar 2020

**HAL** is a multi-disciplinary open access archive for the deposit and dissemination of scientific research documents, whether they are published or not. The documents may come from teaching and research institutions in France or abroad, or from public or private research centers.

L'archive ouverte pluridisciplinaire **HAL**, est destinée au dépôt et à la diffusion de documents scientifiques de niveau recherche, publiés ou non, émanant des établissements d'enseignement et de recherche français ou étrangers, des laboratoires publics ou privés.

# Implementation of an Imaging Spectrometer for Localization and Identification of Radioactive Sources

H. Lemaire<sup>a</sup>, R. Abou Khalil<sup>b</sup>, K. Amgarou<sup>b</sup>, J.-C. Angélique<sup>c</sup>, F. Bonnet<sup>d</sup>,  
D. De Toro<sup>b</sup>, F. Carrel<sup>a</sup>, O. Giarmana<sup>d</sup>, M. Gmar<sup>a</sup>, N. Mena<sup>a,b</sup>, Y. Menesguen<sup>a</sup>,  
S. Normand<sup>a</sup>, A. Patoz<sup>d</sup>, V. Schoepff<sup>a</sup>, P. Talent<sup>d</sup>, T. Timi<sup>b</sup>

<sup>a</sup>CEA, LIST, Gif-sur-Yvette, F-91191, France

<sup>b</sup>CANBERRA, 1 rue des hérons, Saint-Quentin-en-Yvelines, F-78182, France

<sup>c</sup>LPC, 6 boulevard du Maréchal Juin, F-14050, France

<sup>d</sup>CANBERRA, 10 route de Vauzelles, Loches, F-37600, France

**Corresponding author: H. Lemaire, [hermine.lemaire@cea.fr](mailto:hermine.lemaire@cea.fr)**

**Telephone: 0033 1 69 08 35 75**

## Abstract

Spatial localization of radioactive sources is currently a main issue interesting nuclear industry as well as homeland security applications and can be achieved using gamma cameras. For several years, CEA LIST has been designing a new system, called GAMPIX, with improved sensitivity, portability and ease of use. The main remaining limitation of this system is the lack of spectrometric information, preventing the identification of radioactive materials. This article describes the development of an imaging spectrometer based on the GAMPIX technology. Experimental tests have been carried out according to both spectrometric methods enabled by the pixelated Timepix chip used in the GAMPIX gamma camera. The first method is based on the size of the impacts produced by a gamma-ray energy deposition in the detection matrix. The second one uses the Time over Threshold (ToT) mode of the Timepix chip and deals with time spent by pulses generated by charge preamplifiers over a user-specified threshold. Both energy resolution and sensitivity studies demonstrated the superiority of the ToT approach which will consequently be further explored. Energy calibration, tests of different pixel sizes for the Timepix chip and use of the Medipix3 chip are future milestones to improve performances of the newly implemented imaging spectrometer.

## Keywords

**Gamma imaging; GAMPIX; Timepix; imaging spectrometer; Time over Threshold**

## 1. Introduction

Spatial localization of radioactive sources is currently a main issue interesting nuclear industry (nuclear power plants security, decommissioning of nuclear facilities, radiation-protection) as well as homeland security applications (controls, post-accidental interventions)

42 [1] [2]. Gamma imaging is a very interesting technique to achieve this spatial localization by  
43 enabling superimposition of visible and gamma pictures using dedicated devices called  
44 gamma cameras.

45 Spatial localization can be achieved using Compton scattering or coded masks. Compton  
46 approach includes two steps: the scattering of the incident photon and its full absorption.  
47 From the path of each incident photons one can determine cones from which it could have  
48 been emitted. The radioactive source is located at the intersection of all the rebuilt cones. Two  
49 sensors are usually involved in these systems but gamma cameras based on a single sensor  
50 also exist. We can give the example of the recently industrialized Polaris-H system [3] [4]. In  
51 this new gamma camera, the depth of interaction required to determine the path is obtained  
52 from the cathode-to-anode signal ratio (CAR) or from drift time information. Because photons  
53 have to deposit energy in two successive detectors, the Compton approach is mainly dedicated  
54 to photons above 200 keV [3]. In the rest of the article, we will focus on gamma cameras  
55 using coded masks.

56 Current industrial gamma cameras based on coded masks can be considered as first generation  
57 because they are based on scintillator detectors. Much progress was made since the design of  
58 the first gamma camera by Hal Anger (Berkeley University, California) in the last's 50 for  
59 medical applications [5]: digitalization of data processing [6], replacement of the pinholes  
60 used for spatial localization (CARTOGAM, CEA LIST [7]) by multiple hole collimators  
61 (Fixed Multiple hole Collimated Camera, University of Michigan [8]) and MURA coded  
62 masks (RadCam, Radiation Monitoring Devices Inc. [9]), etc. In the 90's, continuous  
63 scintillators moved into pixelated scintillators (CSPD-2, University of Michigan [10]; RMD-  
64 Pinhole, Radiation Monitoring Devices Inc. [11]). At the same time, semiconductor detectors  
65 were developed [6]. Such detectors intended to improve both spatial and energy resolution by  
66 enabling direct conversion from gamma photons to electrical charge. First gamma cameras  
67 integrating semiconductor detectors present some limitations because of small detection  
68 surfaces resulting in small fields of view ([12, 13]) and obligation of cooling the detector  
69 when using materials such as germanium [12]. The progressive development of pixelated  
70 CdTe or CdZnTe substrates hybridized to ASICs [14, 15, 16, 17] opened the way to a second  
71 generation of gamma cameras operating at room temperature.

72 In this context, CEA LIST designed a second generation system, named GAMPIX [1, 18, 19].  
73 GAMPIX's body integrates three main building blocks:

74 The detection system is a 1 mm thick CdTe substrate bump-bonded to a pixelated readout  
75 chip called Timepix [17] and developed by the CERN. In 1.4 cm<sup>2</sup>, the Timepix chip integrates  
76 256 pixels by 256 pixels, 55 μm side, with independent shaping and processing chains.

77 In front of the detection system, the coded mask in tungsten alloy is used as a multi pinhole  
78 collimator for spatial localization [20]. It is characterized by its number of holes (rank) and its  
79 thickness.

80 Finally, the USB module enables plug-and-play connection of the gamma camera with the  
81 acquisition laptop [21] and remote measurements.

82 GAMPIX is currently under industrialization by AREVA CANBERRA (the industrial system  
83 is named iPix, see Fig. 1). Compared to CARTOGAM, which is the current AREVA  
84 CANBERRA industrial system, GAMPIX presents three main improvements:

85 The first one is the low-energy (below 100 keV) sensitivity with a gain of five decades in  
86 comparison with CARTOGAM. GAMPIX is able to detect in 1 s a  $^{241}\text{Am}$  radioactive source  
87 generating a dose rate of  $0.25 \mu\text{Sv}\cdot\text{h}^{-1}$  in the vicinity of the gamma camera. For this reason,  
88 GAMPIX is a performing tool for plutonium detection during decommissioning operations  
89 ( $^{241}\text{Am}$  being a feature of the presence of plutonium). GAMPIX efficiency decreases at high  
90 energy because of both the small detection volume ( $0.1982 \text{ cm}^3$  of CdTe against  $5 \text{ cm}^3$  of  
91 CsI(Tl) for CARTOGAM) and the non-perfect filtering achieved by the coded mask. For this  
92 reason, 20 s are needed to detect a  $^{137}\text{Cs}$  radioactive source with  $2.5 \mu\text{Sv}\cdot\text{h}^{-1}$  dose rate and 60 s  
93 for a  $^{60}\text{Co}$  source giving a dose rate of  $3.8 \mu\text{Sv}\cdot\text{h}^{-1}$ . However, it is important to emphasize that,  
94 by adapting the characteristics of the coded mask, GAMPIX is able to cover an energy range  
95 from  $^{241}\text{Am}$  to  $^{60}\text{Co}$  with better performances than CARTOGAM even at high energy (see [1]  
96 for results obtained in Nuclear Power Plants).

97 The second point is the portability facilitated by the reduction of the weight. CARTOGAM,  
98 which is the lightest system currently on the market, and GAMPIX respectively weight 15 kg  
99 and 2 kg. The difference is mainly due to the shielding required by the scintillation detector of  
100 CARTOGAM.

101 Finally, the third point deals with the ease of use and deployment of GAMPIX in comparison  
102 with CARTOGAM. GAMPIX uses for instance only one cable for camera management, data  
103 transmission and power supply.

104 Besides, GAMPIX has a field of view of  $50^\circ$ . The angular resolution, which refers to the  
105 minimal angle between two radioactive sources to be separated in the decoded image, reaches  
106 down to  $2^\circ$  for a  $^{241}\text{Am}$  radioactive source.

107 GAMPIX applications benefit from its characteristics. Thanks to its great portability, it can  
108 easily be deployed in nuclear power plants in order to control, for instance, the correct  
109 position of lead shielding dedicated to the radiation protection of operators. Regarding nuclear  
110 facilities decommissioning, GAMPIX is able to provide an accurate localization of hot spots  
111 (for instance, in pipes) for targeted decommissioning enabling both reduction of operations  
112 duration and waste volume to be stored. The sensitivity of GAMPIX and its easy deployment  
113 by non-expert end-users enable its use for fast control of luggage (airports) and containers  
114 (ports) for homeland security applications. Finally, for post-accidental interventions,  
115 GAMPIX can help the first responders to quickly identify dangerous areas in Fukushima type  
116 environments. Experimental results illustrating these applications can be found in the  
117 Reference [1].

118 In its current version, the main limitation of the GAMPIX gamma camera is the lack of  
119 spectrometric information, preventing the identification of radioactive material. Thus, dose  
120 rate calculation needs an assumption on the nature of radionuclides and it is impossible to  
121 identify different radionuclides simultaneously present in the environment. Considering this  
122 limitation, it was decided to add new spectrometric capabilities to the GAMPIX gamma  
123 camera to achieve an imaging spectrometer.

124 The Timepix chip offers two approaches for performing spectrometry measurements. The first  
125 one is based on the average size of the clusters which directly depends on the energy of the  
126 incident gamma-ray. As an example, the average cluster size is contained for a given Timepix  
127 energy threshold between 2.8 pixels for a  $^{241}\text{Am}$  source and 7.0 pixels for a  $^{60}\text{Co}$  source. The  
128 incident average energy can thus be deduced from the average cluster size. The second  
129 approach uses the Timepix Time over Threshold (ToT) mode [17, 22, 23]. By setting a  
130 threshold on pulses obtained at the output of charge sensitive preamplifiers, ToT mode  
131 measures the time spent by the pulses over the threshold, which is directly dependent on the  
132 incident gamma-ray energy. Conversion between cluster sizes or ToT values and energy can  
133 be achieved using reference radioactive sources or monoenergetic beams.

134 The purpose of this article is to demonstrate the ability of the GAMPIX system to provide  
135 spectrometric information. Qualitative and quantitative evaluation of its performances  
136 regarding this purpose will be presented. The first part of the document is dedicated to the  
137 preliminary setting of the Timepix chip and to the description of the required analysis tools. In  
138 the second part, methodology for implementing the imaging spectrometer and evaluation  
139 criteria of the final system are presented. Finally, the last part summarizes experimental  
140 results obtained in the frame of this study.

## 141 **2. Settings of the Timepix chip and analysis tools**

142 Fine tuning of the Timepix chip settings was crucial prior the implementation of the imaging  
143 spectrometer. It aims at optimizing both energy resolution and gain. Settings and data  
144 acquisition were performed using the Pixelman interface developed in the Czech Technical  
145 University of Prague [24]. First, threshold equalization with “noise edge” method was carried  
146 out to minimize dispersion around the average threshold value caused by gain differences  
147 between pixels. Then, a parametric study on the thirteen chip parameters showed that the  $I_{krum}$   
148 DAC had the greatest influence on both energy gain and energy resolution [25]. The  $I_{krum}$   
149 current both controls falling times of pulses generated by charge preamplifiers and  
150 compensates leakage currents (within the limit of  $I_{krum}/2$ ). All parameters were finally set to  
151 their default value, except  $I_{krum}$  which was set to the DAC code value 2 corresponding to a  
152 falling time in the order of  $1\ \mu\text{s}$  [26]. It is important to notice that the pile-up is limited with  
153 such a value. The substrate bias voltage has to be high enough (in absolute value) to minimize  
154 charge spreading and charge trapping which is a drawback of CdTe. In our case, bias voltage  
155 was set to  $-110\ \text{V}$ . Conversion between ToT values and energy can be done by mean of a  
156 calibration curve [27-28]. This curve is mostly linear, except at very low energy (just above  
157 the threshold set on the pulses). Energy calibration also aims at optimizing energy resolution  
158 by correcting the shift between peaks due to clusters of different sizes (Fig. 2). In this study,  
159 we tested our imaging spectrometer without energy calibration but directly with ToT values.  
160 It is important to emphasize on the fact that energy resolution improvement given by the  
161 energy calibration step was not crucial for these measurements because gamma-ray spectra  
162 coming from the different studied radionuclides have a typical signature (Table I).

163 Data processing was performed with dedicated MATLAB software developed by CEA LIST.  
164 This software implements processing functions dealing with both spectrometric approaches

165 tested in the imaging spectrometer. Concerning cluster size, the software identifies clusters as  
166 set of neighboring pixels. A maximal allowed cluster size can be set by the user to remove  
167 cosmic rays, size of which commonly exceeds 20 pixels. It is important to set a low enough  
168 acquisition time per frame to avoid pile-up which would lead to non-physical clusters  
169 resulting from the sum of successive close events. Cluster size histograms giving the number  
170 of occurrences depending on the cluster size are finally plotted. As far as ToT mode is  
171 concerned, the software sums ToT values of all pixels forming a cluster. If energy calibration  
172 has been achieved, energy conversion is done before summation. Spectra giving the number  
173 of occurrences as a function of ToT values are finally plotted. The software also achieves  
174 spatial reconstruction from the coded mask projection on the detection matrix. Spatial  
175 reconstruction can be focused on a given cluster size windowing or ToT windowing specified  
176 by the user. This functionality will be used for the implementation of the imaging  
177 spectrometer as presented in section III.

### 178 **3. Implementation of the imaging spectrometer and evaluation criteria**

179 To demonstrate the feasibility of an imaging spectrometer based of the GAMPIX gamma  
180 camera, it was decided to develop a device achieving a selective spatial reconstruction  
181 depending on the energy of incident photon (via cluster size and ToT values). This device was  
182 tested with four radioactive sources covering the energy range of interest for the GAMPIX  
183 system (see Table I). Performances of both spectrometric approaches in terms of  
184 discrimination capability, and comparison with the GAMPIX gamma camera in its current  
185 version in terms of sensitivity were assessed. The first part of this section is dedicated to the  
186 methodology used for the implementation of the imaging spectrometer while the second part  
187 justifies the choice of evaluation criteria.

#### 188 **3.1 Implementation of the imaging spectrometer**

189 Implementation of the imaging spectrometer according to both cluster size and ToT values  
190 approaches is based on windowing. Cluster size windowing requires a preliminary  
191 measurement with each radionuclide taken alone. From the cluster size histograms, mean  
192 cluster size, dispersion around the mean and overlapping between radionuclides are evaluated.  
193 The first spatial reconstruction is performed on the single mean cluster size. Then, the  
194 windowing is progressively broadened and the best configuration is determined by  
195 qualitatively evaluated spatial reconstructions. To appreciate differences between cluster size  
196 histograms, Fig. 3 shows histograms of  $^{241}\text{Am}$  and  $^{60}\text{Co}$  radioactive sources and Table II gives  
197 mean cluster size and percentage of clusters in different ranges for the four radionuclides  
198 tested. Table III summarizes the cluster size windowing chosen for best discrimination. To  
199 avoid overlapping between radionuclides, mean cluster size and most frequent cluster sizes  
200 are not necessarily included in the windowing.

201 Concerning ToT windowing, a preliminary measurement with each radionuclide taken alone  
202 is also required to identify in the spectra ToT values associated with typical features  
203 (photoelectric peaks, Compton edge, etc.) Spectra obtained with each radionuclide are then  
204 compared to determine if there is overlapping due to the energy resolution of the sensor. The

205 first windowing is centered on typical features and the best windowing is finally obtained by  
206 sequential approach. Typical features of the four radionuclides studies and position of the  
207 windowing are shown in Fig. 4. All ToT spectra obtained are in good agreement with  
208 previous literature results [27] and show the ability of the ToT mode to provide useful  
209 gamma-ray spectra, even at high energy ( $^{137}\text{Cs}$  and  $^{60}\text{Co}$ ). One can notice the large fraction of  
210 events on the fluorescence and escape peaks. It is explained by the pixelation of the detector:  
211 it is unusual that both incident photon and fluorescence photon deposit their energy in the  
212 same 55- $\mu\text{m}$ -side pixel. Table IV summarizes ToT windowing for all tested radionuclides.  
213 Because of overlapping, windowing does not necessarily include typical features.

### 214 **3.2 Evaluation criteria**

215 The first evaluation criterion of imaging spectrometer performances is the discrimination  
216 ability, which is qualitatively evaluated from spatial reconstructions. If radionuclides with  
217 different gamma-ray emissions are simultaneously present in the field of view, the  
218 discrimination ability characterizes the ability of the system to reconstruct only radioactive  
219 sources included in a given energy range.

220 The second evaluation criterion is the sensitivity, which corresponds to the minimal duration  
221 required for detecting a radionuclide inducing a given dose rate near the gamma camera. The  
222 sensitivity corresponds to a picture free of artifacts, as shown in Fig. 5 (b). Three parameters  
223 have a great impact on the sensitivity. The first one is the detector efficiency. It decreases  
224 when the incident gamma-ray energy increases as shown in Fig. 6. For a 1-mm-thick CdTe  
225 detector, efficiency drastically decreases from 100 keV. The second factor is the coded mask  
226 and its characteristics. A tradeoff has to be found between thickness (sensitivity) and number  
227 of holes (i.e. the rank, which defines the angular resolution). The last factor is the energy  
228 windowing. Without windowing (standard working mode for the GAMPIX gamma camera),  
229 all photons hitting the detector are taken into account. The narrower windowing is, the fewer  
230 photons are considered, and the more sensitivity is decreased.

## 231 **4. Performances of the imaging spectrometer**

232 Performances according to both evaluation criteria presented in section III are successively  
233 presented. All acquisitions were performed in “Time over Threshold” mode and in “frame”  
234 type with 1 s acquisition per frame. They were repeated three times to control reproducibility.

### 235 **4.1 Discrimination ability**

236 To evaluate discrimination capability, radioactive sources were disposed two or three at a  
237 time in front of the gamma camera over a graduated table. Tests were carried out for distance  
238 between radioactive sources and GAMPIX gamma camera varying between 50 cm and  
239 150 cm on the camera axis and between 0 and 50 cm on each side of the camera on the  
240 perpendicular axis. Acquisition time was set between 300 s and 2000 s depending on  
241 configurations tested.

242 Table V shows pictures obtained after both cluster size windowing and ToT windowing for a  
243 1500 s acquisition with  $^{241}\text{Am}$ ,  $^{133}\text{Ba}$  and  $^{137}\text{Cs}$  radioactive sources positioned in the  
244 configuration illustrated in Fig. 7. Both approaches are efficient for  $^{241}\text{Am}$  and  $^{137}\text{Cs}$   
245 discrimination but cluster size windowing is unable to separate  $^{133}\text{Ba}$  from  $^{241}\text{Am}$ .  $^{137}\text{Cs}$  also  
246 appears less punctual for cluster size configuration and there are more artifacts on  $^{241}\text{Am}$   
247 picture. All tested configurations proved the superiority of ToT approach on cluster size  
248 approach regarding this evaluation criterion.

249 Three factors explain this superiority. First, spectra of the four radionuclides tested are well  
250 differentiated contrary to cluster size plots: centroid of photoelectric peaks varies from about  
251 500 to 4500 from  $^{241}\text{Am}$  to  $^{60}\text{Co}$  (Fig. 4), while mean cluster size only changes from about 3  
252 to 7 (Table III). Secondly, the 11810 channels of the counting system in ToT mode are great  
253 enough to show these differences. Finally, ToT mode enables to carry out fine spectrometry  
254 measurements while cluster size mode only deals with mean energy values.

## 255 **4.2 Sensitivity**

256 During our experiments, sensitivity was determined for each source placed at 1 m from the  
257 gamma camera in the camera axis, without windowing, with cluster size windowing and with  
258 ToT windowing. Several configurations of the mask were tested. We were looking for the loss  
259 of sensitivity induced by the spectro-imaging mode for both spectrometric approaches with  
260 respect to the GAMPIX gamma camera in its current version.

261 Tables VI to VIII summarize sensitivity for all radionuclides tested without windowing  
262 (GAMPIX gamma camera in its current version) and with cluster size and ToT windowing for  
263 several configurations of the coded mask. Percentages below the values indicate the loss of  
264 sensitivity due to both windowing techniques.

265 Several conclusions can be drawn from these results. Concerning coded masks, the one of  
266 rank 7 with a thickness of 4 mm produces best results for energies under 100 keV ( $^{241}\text{Am}$ ,  
267  $^{133}\text{Ba}$ ), while mask of rank 7 with a thickness of 8 mm is more efficient for higher energies  
268 ( $^{137}\text{Cs}$ ,  $^{60}\text{Co}$ ). Rank 13 offers better performances than rank 7 in terms of spatial resolution but  
269 is less efficient in terms of sensitivity. Two millimeters appears to be a too-thin thickness for  
270 each of the tested radionuclides, especially for high-energy gamma-ray emissions. In the case  
271 of unknown searched radionuclides, coded mask of rank 7 with a thickness of 4 mm offers the  
272 best tradeoff.

273 Concerning energy windowing, it causes a loss of sensitivity greater than 20% in most cases,  
274 which is explained by the little fraction of events occurring in the sensor and finally selected  
275 for spatial reconstruction. For low energies, this sensitivity loss is not a real problem because  
276 of very small acquisition times required by the GAMPIX gamma camera (from 1 s to 2 s for  
277  $^{241}\text{Am}$  with rank 7 and thickness of 8 mm for the coded mask). For higher energies, loss can  
278 be limited by the choice of the most adapted mask. Best sensitivities are obtained for ToT  
279 windowing in comparison with cluster size windowing. Degraded results with  $^{60}\text{Co}$  are  
280 explained by photoelectric peak spreading due to the high mean cluster size (7) and to the  
281 dispersion around this value which causes shifts between photoelectric peaks.



282

## 5. Conclusion and outlook

283 The purpose of our study was to demonstrate the feasibility of an imaging spectrometer based  
284 on the GAMPIX gamma camera and to evaluate its performances. Two methods were tested  
285 to implement this imaging spectrometer: cluster size and ToT approaches. Tests on  
286 discrimination ability and sensitivity both proved the feasibility of such a device and the  
287 superiority of ToT approach. Loss of sensitivity with ToT approach is greater than 20%. If it  
288 is not a problem for low energies, a relevant choice of the mask can mitigate this drawback  
289 for energies higher than 100 keV. If the radionuclide is unknown, the coded mask of rank 7  
290 with a thickness of 4 mm offers the best compromise.

291 Further developments of the imaging spectrometer will combine both cluster size and ToT  
292 spectrometric approaches. Next planned step is the integration of the energy calibration in the  
293 imaging spectrometer for the analysis of closer gamma-ray energies. Because of the high  
294 mean cluster size, improvements are also expected for high energies ( $^{60}\text{Co}$ ). Energy  
295 calibration measurements should take place at the SOLEX facility which provides  
296 monoenergetic beams from 0.5 keV to 28 keV [30]. As a first step, we plan the global  
297 calibration of the Timepix chip. Improvements of the energy resolution of a factor between  
298 two and four are reported by [26] with a pixel by pixel calibration and this approach will be  
299 considered as a second step. Test of a 1 mm thick, 110  $\mu\text{m}$  pixel side Timepix chip is also  
300 expected. It would enable to evaluate the energy resolution gain due to the limitation of  
301 charge sharing between several pixels, which is one of the main explanations for energy  
302 resolution degradation.

303 Finally, the replacement of the Timepix chip by a Medipix3 chip will be studied. The ToT  
304 mode is not implemented in the Medipix3 chip and spectra have to be obtained by counting  
305 the number of events for each threshold value [31]. The main improvement compared to  
306 previous Medipix chips concerns the hardware connection between several neighboring  
307 pixels, which should drastically improve the energy resolution of the system.

308

## 309 References

310

311 [1] F. Carrel, et al., "GAMPIX: a New Gamma Imaging System for Radiological Safety and  
312 Homeland Security Purposes", *IEEE NSS Conference Record*, 2011.

313 [2] V. Schoepff, et al., "BOOSTER: Development of a Toolbox for Triage of Large Group of  
314 Individuals Exposed to Radioactive Material", accepted for publication in *IEEE*  
315 *Transactions on Nuclear Science*, 2014.

316 [3] W. Kaye, et al., "Calibration and Operation of the Polaris 18-Detector CdZnTe Array",  
317 *IEEE*, 2010.

318 [4], "Polaris-H Gamma-Ray Imaging Spectrometer", *presentation brochure*.

319 [5] H.O. Anger, "Scintillation Camera", *The review of scientific instruments*, vol. 29, num. 1,  
320 1958.

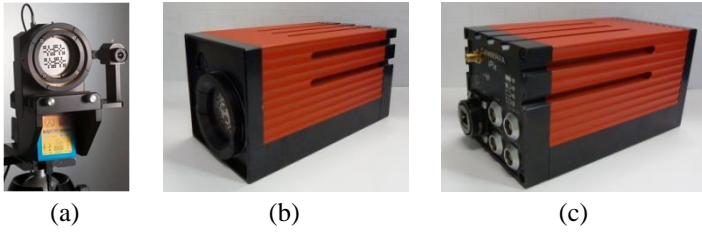
321 [6] M. Ricard, "Imaging of gamma emitters using scintillation cameras", *Nucl. Instrum.*  
322 *Methods Phys. Res. A*, vol. 527, pp. 124-129, 2004.

- 323 [7] O. Gal, et al., “CARTOGAM – a portable gamma camera for remote localization of  
324 radioactive sources in nuclear facilities”, *Nucl. Instrum. Methods Phys. Res. A*, vol. 460,  
325 pp. 138-145, 2001.
- 326 [8] S.V. Guru, et al., “A high energy gamma camera using a multiple hole collimator and  
327 PSPMT”, *Nucl. Instrum. Methods Phys. Res. A*, vol. 353, pp. 328-333, 1994.
- 328 [9] M. Woodring, et al., “Advanced radiation imaging of low-intensity gamma-ray sources”,  
329 *Nucl. Instrum. Methods Phys. Res. A*, vol. 422, pp. 709-712, 1999.
- 330 [10] Z. He, et al., “The CSPD-2 Gamma-Ray Imaging System”, *IEEE TNS*, vol. 44, num. 3,  
331 1997.
- 332 [11] R. Redus, et al., “A combined video and gamma ray imaging system for robots in nuclear  
333 environments”, *Nucl. Instrum. Methods Phys. Res. A*, vol. 353, pp. 324-327, 1994.
- 334 [12] V.R. McCready, et al., “Clinical tests on a prototype semiconductor gamma-camera”,  
335 *British Journal of Radiology*, vol. 44, pp. 58-62, 1971.
- 336 [13] Y. Eisen, et al., “A gamma camera based on CdTe detector”, *Nucl. Instrum. Methods  
337 Phys. Res. A*, vol. 380, pp. 474-478, 1996.
- 338 [14] Z. He, et al., “3-D position sensitive CdZnTe gamma-ray spectrometers”, *Nucl. Instrum.  
339 Methods Phys. Res. A*, vol. 422, pp. 173-178, 1999.
- 340 [15] C. Mestais, et al., “A new design for a high resolution, high efficiency CZT gamma  
341 camera detector”, *Nucl. Instrum. Methods Phys. Res. A*, vol. 458, pp. 62-67, 2001.
- 342 [16] O. Limousin, et al., “Caliste 256: A CdTe imaging spectrometer for space science with a  
343 580  $\mu\text{m}$  pixel pitch”, *Nucl. Instrum. Methods Phys. Res. A*, vol. 647, pp. 46-54, 2011.
- 344 [17] X. Llopert, et al., “Timepix, a 65k programmable pixel readout chip for arrival time,  
345 energy and/or photon counting”, *Nucl. Instrum. Methods Phys. Res. A*, vol. 581, pp. 485-  
346 494, 2007.
- 347 [18] M. Gmar, et al., “GAMPIX: a new generation of gamma camera”, *Nucl. Instrum.  
348 Methods Phys. Res. A*, Vol. 652, pp. 638-640, 2011.
- 349 [19] F. Carrel, et al., “GAMPIX: a new generation of gamma camera for hot spot  
350 localisation”, *Proceedings of the ISOE Conference*, Cambridge, 2010.
- 351 [20] S. R. Gottesman and E. E. Fenimore, “New family of Binary Arrays for Coded Aperture  
352 Imaging”, *Applied Optics*, Vol. 28, n. 20, pp. 4344-4352, 1989.
- 353 [21] Z. Vykydal, “Microprocessor controlled USB interface for Medipix2 detector”, *Ph.D.  
354 dissertation*, Department of Physical Electronics, Czech Technical University, Prague,  
355 Poland, 2004-2005.
- 356 [22] D. Maneuski, et al., “Imaging and spectroscopic performance studies of pixelated CdTe  
357 detector”, *Journal of Instrumentation*, vol. 7, 2012.
- 358 [23] E. Fröjdh, et al., “X-ray absorption and charge transport in a pixelated CdTe detector  
359 with single photon processing readout”, *Journal of Instrumentation*, Vol. 7, 2011.
- 360 [24] D. Turecek, et al., “Pixelman: a multi-platform data acquisition and processing software  
361 package for Medipix2, Timepix and Medipix3 detectors”, *IOP*, 2011.
- 362 [25] M. Kroupa, et al., “Optimization of the spectroscopic response of the Timepix detector”,  
363 *IOP*, 2011.
- 364 [26] M. Filipenko et al., “Characterization of the energy resolution and the tracking  
365 capabilities of a hybrid pixel detector with CdTe-sensor layer for a possible use in a  
366 neutrinoless double beta decay experiment”, *Eur. Phys. J. C*, 73:2374, 2013.

- 367 [27] J. Jakubek, “Precise energy calibration of pixel detector working in time-over-threshold  
368 mode”, *Nucl. Instrum. Methods Phys. Res. A*, vol. 633, pp. S262-S266, 2011.
- 369 [28] D. Turecek, et al., “Energy calibration of pixel detector working on Time-Over-  
370 Threshold mode using test pulses”, *NSS/MIC ISSN 1082-3654*, pp. 1722-1725, 2011.
- 371 [29] C. Ponchut and M. Ruat, “Energy calibration of a CdTe X-ray pixel sensor hybridized to  
372 a Timepix chip”, *IOP*, 2012.
- 373 [30] Y. Ménesguen and M.C. Lépy, “Efficiency calibration and surface mapping of an  
374 energy-dispersive detector with SOLEX: a compact tunable monochromatic X-ray  
375 source”, *Nucl. Instrum. Methods Phys. Res. A*, vol. 695, pp. 193-196, 2012.
- 376 [31] R. Ballabriga et al., “Medipix3:A 64 k pixel detector readout chip working in single  
377 photon counting mode with improved spectrometric performance”, *Nucl. Instrum.*  
378 *Methods Phys. Res. A*, vol. 633, pp. S15-S18, 2011.

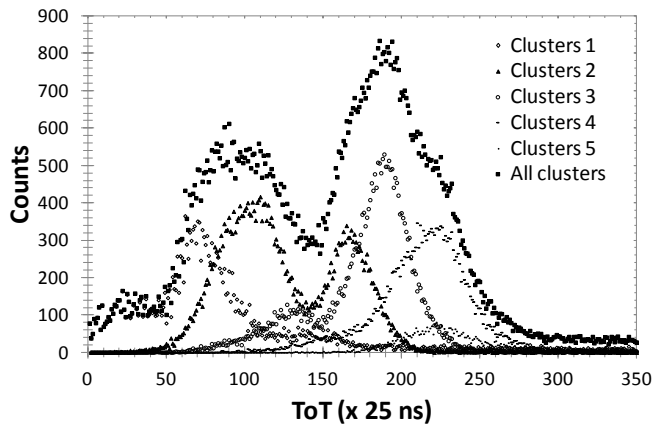
379 **Figures**

380



381 Fig. 1: (a) GAMPIX gamma camera prototype developed by CEA LIST (b) front side and (c) back side of the  
382 iPix industrial prototype developed by CANBERRA.

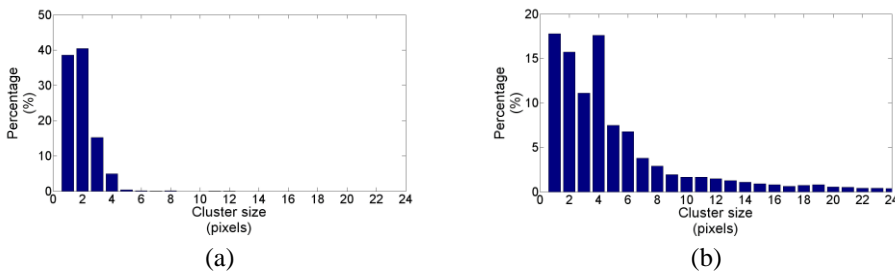
383



384

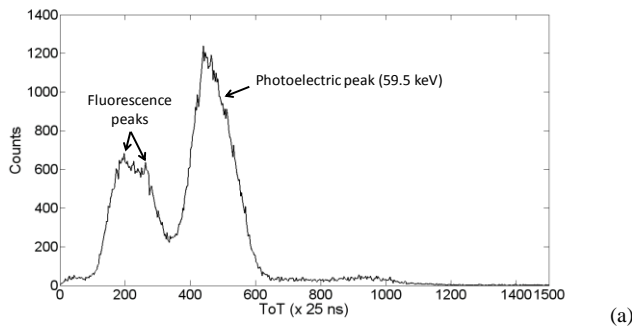
385 Fig. 2: Spectra obtained with a  $^{241}\text{Am}$  radioactive source depending on cluster size.

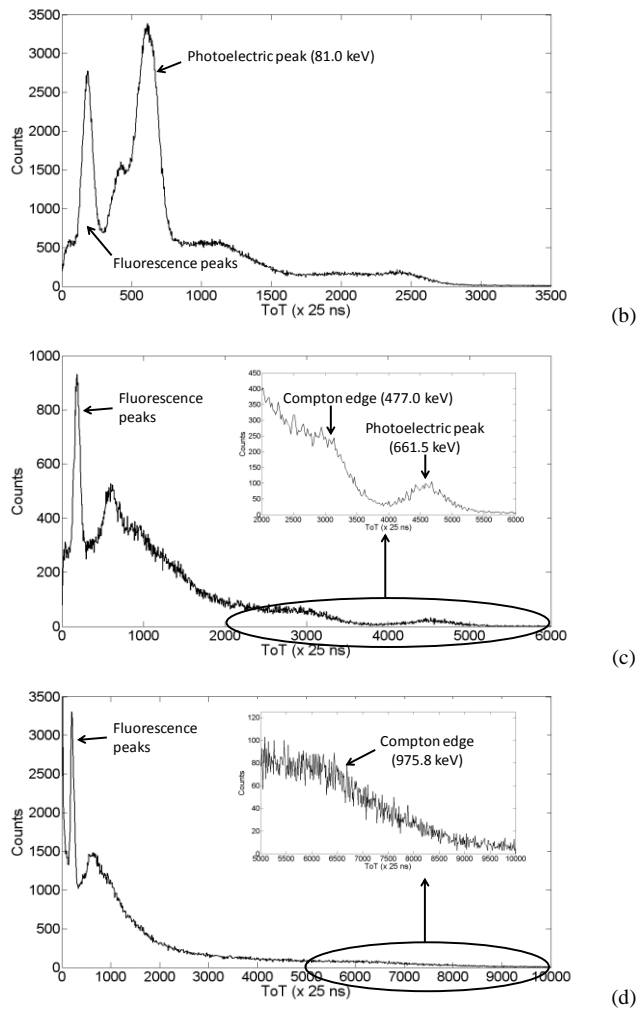
386



387 Fig. 3: Cluster size histograms for (a)  $^{241}\text{Am}$  and (b)  $^{60}\text{Co}$

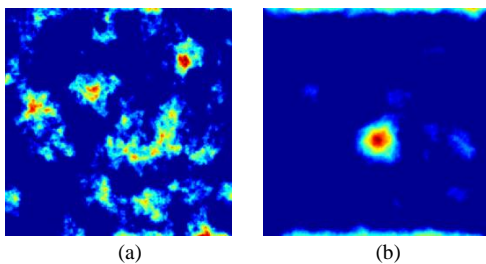
388





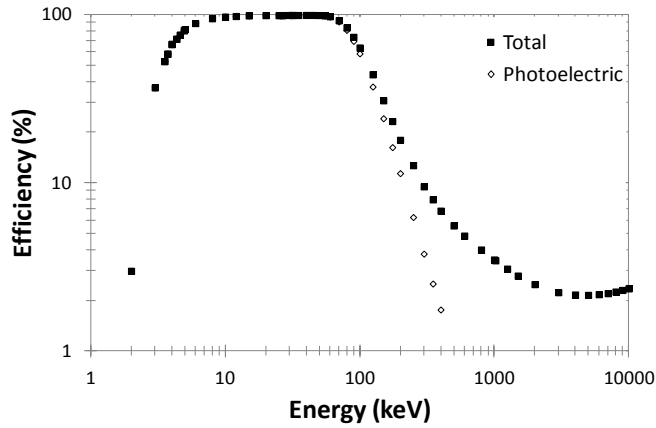
389 Fig. 4: Spectra of (a)  $^{241}\text{Am}$ , (b)  $^{133}\text{Ba}$ , (c)  $^{137}\text{Cs}$  and (d)  $^{60}\text{Co}$  with typical features.

390

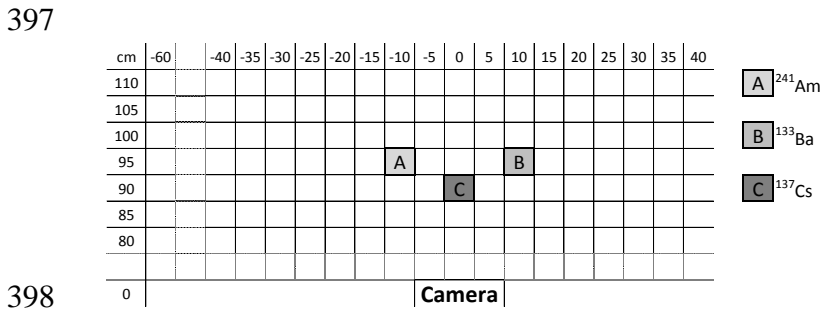


391 Fig. 5: Spatial reconstruction of a radioactive source of  $^{137}\text{Cs}$  (coded mask of rank 7 with thickness of 4 mm) for  
 392 acquisition time of (a) 10 s and (b) 400 s. The presence of artifacts can be observed on the left. Result obtained  
 393 for a 400 s acquisition time is considered as satisfying.

394



395  
396 Fig. 6: Logarithmic plot of efficiency for 1 mm CdTe detector between 1 keV and 10 MeV.



398  
399 Fig. 7: Example of the experimental configuration used to evaluate both spectrometric approaches. Workbench  
400 on which radioactive sources are placed is seen from above.

401  
402 Tables

403  
404  
405

Table 1  
Characteristics of radioactive sources tested

Source	<sup>241</sup> Am	<sup>133</sup> Ba	<sup>137</sup> Cs	<sup>60</sup> Co
Energy (keV)	59.5	[81.0, 356.0]	661.7	1173.2 and 1332.5
Activity (MBq)	72.8	35.1	26.1	11.7
Dose rate at 1 m (μSv/h)	0.286	1.658	1.987	3.585

406  
407  
408

Table 2  
Mean cluster size and cluster size probabilities

Radionuclide	Mean cluster size (pixels)	Cluster size probability (%)		
		0-4	4-10	> 10
<sup>241</sup> Am	2.8	90.1	9.8	0.1
<sup>133</sup> Ba	3.9	70.4	28.4	1.2
<sup>137</sup> Cs	4.4	59.9	35.4	4.7
<sup>60</sup> Co	7.0	54.6	30.8	14.6

409  
410  
411

Table 3  
Cluster size windowing

Radionuclide	Windowing (cluster size)	Mean cluster size (pixels)
<sup>241</sup> Am	0-3	2.8
<sup>133</sup> Ba	7-10	3.9
<sup>137</sup> Cs	10-100	4.4
<sup>60</sup> Co	12-100	7.0

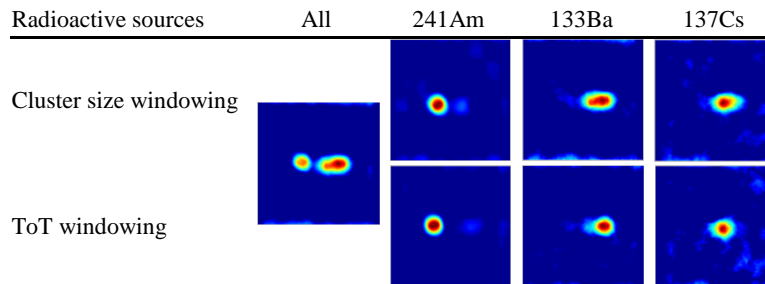
413  
414

Table 4  
ToT windowing

Radionuclide	Windowing (ToT values)
<sup>241</sup> Am	400-500
<sup>133</sup> Ba	600-800
<sup>137</sup> Cs	1000-2000
<sup>60</sup> Co	5000-15000

415  
416  
417

Table 5  
Mean cluster size and cluster windowing



418  
419  
420  
421

Table 6  
Sensitivities without windowing and for cluster size and ToT windowing with rank 7, thickness of 4 mm coded mask

	Without windowing	Cluster size windowing	ToT windowing
<sup>241</sup> Am	1 s	1 s 0%	<b>1 s</b> <b>0%</b>
<sup>133</sup> Ba	4 s	15 s +275%	<b>7 s</b> <b>+75%</b>
<sup>137</sup> Cs	60 s	130 s +117%	100 s +67%
<sup>60</sup> Co	300 s	400 s +33%	1500 s +400%

422  
423  
424  
425

Table 7  
Sensitivities without windowing and for cluster size and ToT windowing with rank 7, thickness of 8 mm coded mask

	Without windowing	Cluster size windowing	ToT windowing
<sup>241</sup> Am	1 s	2 s +100%	2 s +100%
<sup>133</sup> Ba	10 s	25 s +150%	12 s +20%
<sup>137</sup> Cs	20 s	180 s +800%	<b>80 s</b> <b>+300%</b>
<sup>60</sup> Co	60 s	<b>125 s</b> <b>+108%</b>	650 s +983%

426  
427  
428

429  
430  
431

Table 8  
Sensitivities without windowing and for cluster size and ToT windowing with rank 13, thickness of 2 mm coded mask

	Without windowing	Cluster size windowing	ToT windowing
<sup>241</sup> Am	3 s	4 s +33%	4 s +33%
<sup>133</sup> Ba	14 s	100 s +614%	17 s +21%
<sup>137</sup> Cs	300 s	> 600 s > +100%	> 600 s > +100%
<sup>60</sup> Co	Not visible	Not visible	Not visible

432